# 36. Investigating the contact dynamics between tool and granular material using Distinct Element Method (DEM)

○ Ha H. BUI, *Graduate School of Science and Engineering, Ritsumeikan University*
Ryoichi FUKAGAWA, *Department of Civil Engineering, Ritsumeikan University*

**Abstract:**
The contact dynamics between tool and granular material is presented in this study using numerical simulation. We focus on the failure mechanism and the resistance force acting on the cutting-tool during the excavation process. Our numerical simulations are performed in both two and three dimensional directions and compared with the 2D experimental model, which is carried out using aluminum bars regarding as soil model. This research has showed that DEM simulation results are well fitted in experiment in both mean of shear deformation pattern and the resistance force acting on the cutting-tool. The force has big fluctuation and the fluctuation is directly proportional to the granular size. In spite of fluctuation, the mean force is independent of particles size. The development of slip surface in 2D and the 3D failure mechanism during the excavation process could be visualized clearly through the DEM simulation.

*Keyword: Distinct Element Method (DEM), excavation, granular material, cutting-tool, rake angle*

## 1. INTRODUCTION:

Recently, numerical simulation of granular material such as soil mechanics and silo engineering is usually using the Distinct Element Method which was developed by Cundall and Strack [1] in 1979. In this method, the granular material is modeled by circular particles (possible for irregular shape) and each couple of particles is connecting by a spring-dashpot model in both normal and shear directions as shown in Fig.1. The contact between two particles will then be described by a suitable contact model. This method has provided an excellent way to model the behavior of granular material.

This paper concerns a numerical investigation of an action of a rigid "tool" upon a granular material (excavation process). In 2D simulation investigation, the cutting-tool was first set on outside of a granular bin composed of irregular circle particles initially in equilibrium under gravity in side a rectangular box. After that, this tool was forced to move horizontally with a constant speed. This simulation was then extended into 3D simulation in which the spherical particles are assumed to be soil model.

We focuses on the total force acting on the cutting-tool and the shear deformation pattern of soil generating in front of the tool. In general, the resistance force acting on the tool can be calculated based on the passive earth pressure theory. However, several researchers have indicated that the actual resistance force is overestimated comparing with the theoretical value [2, 4]. This problem is considered due to the lack information of soil failure generating in front of the cutting-tool. Therefore it is necessary to clarify this failure mechanism.

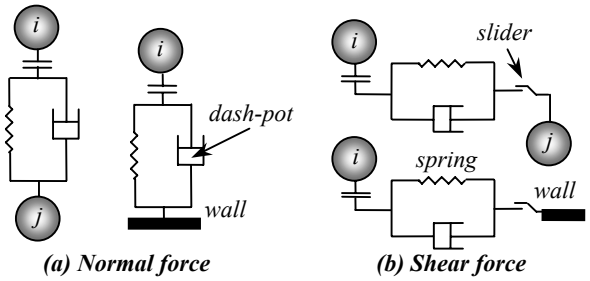


*Fig.1: Models of contact force in normal and shear direction*

Our research reveals a big fluctuation in force acting on the cutting-tool and this fluctuation is proportional to the grain size. In spite of fluctuation, its mean value is independent of grain size. In 2D, this force tends to increase linearly with respect to the excavation progress, but in 3D this force seems to be constant after reaching a maximum value.

In the means of the failure mechanism, our simulation showed that the slip surface of soil failure is become curve and it is enlarged from the tool tip to the ground surface. The volume of 3D failure could be clarified in our simulation. The main results will be presented after the short description of the simulation method and of physical parameters for our simulation systems. Several aspects of the problem such as the influence of grain size, of the angle of the tool (rake angle) and of the cutting speed will also be discussed through this paper.

## 2. SIMULATION METHOD

For these simulations, we have developed our computer program based on the method proposed by

Cundall & Strack [1] so called Distinct Element Method. For a detailed description of this method the reader may refer to [2, 3]. In our simulation granular particles are assumed to be an assembly of circle disks in 2D and spherical ones in 3D. These particles contact each other at a contact point which is modeled by a spring-dashpot model, as shown in Fig.1, in both normal and shear directions. Using this model, the forces acting on particle including normal force and friction force could be calculated. The friction force in shear direction is then modeled to satisfy the Coulomb's friction law and finally the motion of particle will be solved by taking integration of the motion equations.

As mentioned above, in 2D simulations we used the circular particles. These particles are generated randomly in a rectangular box. Before starting a numerical simulation, one needs to compact the particles to a relax condition which has sufficiently small kinetic energy. The cutting-tool in this simulation consists of a rectangular rod enveloped by a circle particle in order to make the tool tip smoother. Since we are mainly interested in the failure pattern and the resistance force acting on the cutting-tool, the tool was initially set outside of the soil box at a desired depth as near as possible to the granular sample. Then this tool was pushed horizontally with a constant speed along the granular bed. Most of simulations were performed with speed of 2cm/s. Few of them, however, were performed with 1cm/s in order to compare with experiments. For the simulation with the cutting speed of 2cm/s, we used distributed radius particles. Four samples with different particles size are simulated in order to check the effect of particle size on the force fluctuation, these samples are listed in Table 1 as A, B, C, and D. Simulation with the cutting speed of 1cm/s used only two kinds of particles with diameter of 1.5mm and 3mm (sample F). This simulation will then be compared with an experiment using the same particle radius, excavation speed, excavation depth and void ratio. A detailed description of experiment will be described later.

In 3D simulation, the particles configuration are also generating some what similar to the 2D problem. Particles were also first generated randomly into a cubic-rectangular soil bin (120×120×120) mm, then they are compacted by gravity to the height of 50mm until the particle system is stable. The cutting-tool, which has width of 40mm, consists of a cubic-rectangular rod with smoothed surfaces and spherical edges. Initially, this tool was set on outside of the soil box at the depth of 30mm as near as possible to the granular sample, after that the tool is moved horizontally with a constant speed of 2cm/s. We also considered the effect of the rake angle on the soil failure and resistance force by performing two simulations with rake angle of 90 degree (sample G) and 60 degree (sample H) comparing with the horizontal direction. The control diameters and void ratio in 3D simulation are distributed in Table 1 as sample G, H. The coefficient of internal friction equals 0.3 for both 2D and 3D. The walls in all simulations are treats as frictionless and the coefficient of friction between free particles and tool is 0.3.

*Table 1*. Characteristics of the samples.

| Samples | No. of particles | Control diameter (mm) | Initial void ratio |
|---|---|---|---|
| A | 8585 | $2.8 \le d \le 3.6$ | 0.1954 |
| B | 3819 | $4.0 \le d \le 5.4$ | 0.1963 |
| C | 1628 | $6.2 \le d \le 8.2$ | 0.1928 |
| D | 1008 | $8.2 \le d \le 10.1$ | 0.1947 |
| F | 7450 | $d = 1.5; d = 3$ | 0.1485 |
| G | 51840 | $2.0 \le d \le 3.0$ | 0.2125 |
| H | 51840 | $2.0 \le d \le 3.0$ | 0.2231 |

In order to validate our simulation results, 2D experiments were performed in this study. In this experiment aluminum bars, which have 1.5 and 3mm in diameter and 50mm in length, were used regarding as granular material. Aluminum bars were distributed randomly into a soil box to the height of 14cm and the cutting-tool was immerged 8cm depth into sample. A 6-axis force sensor was attached behind the cutting-tool in order to measure the resistance force and moment acting on the cutting-tool. And a high speed camera was used to record the failure deformation pattern of the sample during the excavation process. The excavation was done by dragging the soil box to the left directions with a speed of 1cm/s. The experimental apparatus using in this study are shown in the Fig.2.

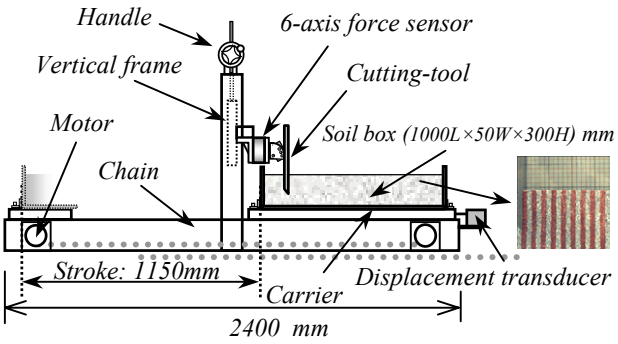

*Fig.2: Two dimensions experimental apparatus*

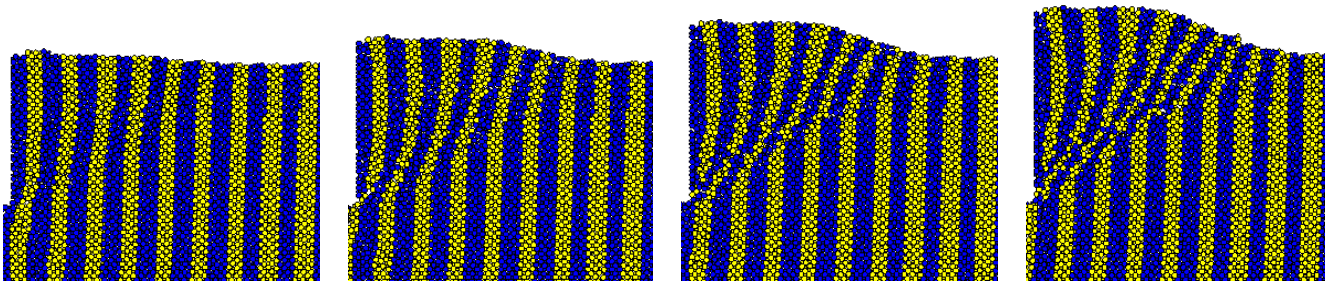

*10mm displacement* *20mm displacement* *30mm displacement* *40mm displacement*

(a) Excavation progress in simulation using DEM (2D simulation)

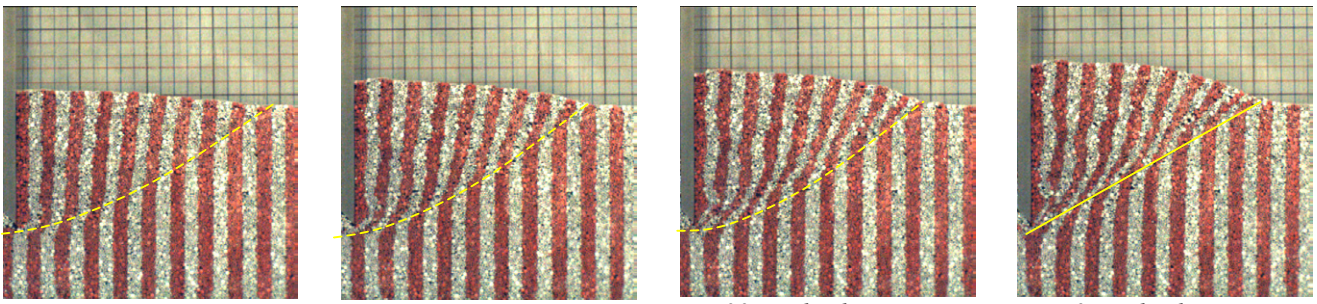

*10mm displacement* *20mm displacement* *30mm displacement* *40mm displacement*

(b) Excavation progress in experiment (2D experiment)

*Fig.3: The comparison of soil deformation pattern between simulation and experiment*

## 3. RESULTS AND DISCUSSION:

### *3.1. Shear deformation and resistance force in 2D*

Fig.3 shows the comparison between experiment and simulation results in term of the shear deformation pattern, each image was taken after 10mm displacement of the cutting-tool. Fig.3 (a) showed the simulation results while Fig.3 (b) showed the experimental one. From this figure it could be seen that the shear deformation pattern in simulation agreed very well with the experimental results. The slip line, boundary between moving soil volume and stationary soil volume, changes from curve line into straight line after each cycle where a new slip line is generated. The mechanism of this phenomenon can be explained due to the superposition of the soil mass in front of the cutting-tool.

The agreement between simulation and experiment is not only in term of shear deformation pattern but also in term of the excavation resistance acting on the tool as shown in Fig.4. In this figure, the simulation result is compared with three experimental results which were performed in the same condition. The result has shown that in both simulation and experiments, the force acting on the cutting-tool have big fluctuations. This fluctuation was caused by some reasons, one could be the magnitude of particles size and the other reason could be the effect of non-cohesion material using in both simulation and experiment. In spite of fluctuation, this force seems to increase linearly with respect to the traveling distance of the cutting-tool.

In order to verify the effect of the particles size on the fluctuation of resistance force, we have performed four simulations using different size of particles corresponding to samples (A-D) as shown in Table 1.

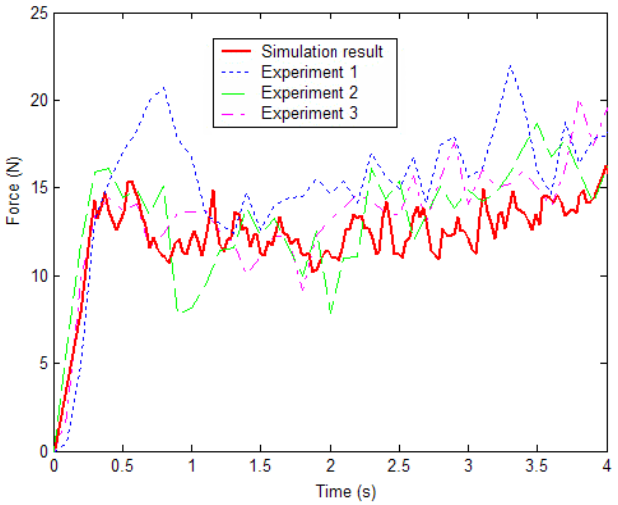


*Fig.4: Horizontal component force acting on the cutting-tool as a function of time in experiment (dash lines) and simulation (solid line).*

Fig.5 shows the results of the horizontal resistance force acting on the cutting-tool in simulations corresponding to different size particles simulation (samples A to D). From this figure, it could be seen that the force fluctuation reduces as the size of particle decreases. In spite of the fluctuation, the mean force is almost the same in all of simulations and this mean force increases linearly with respect to the time.

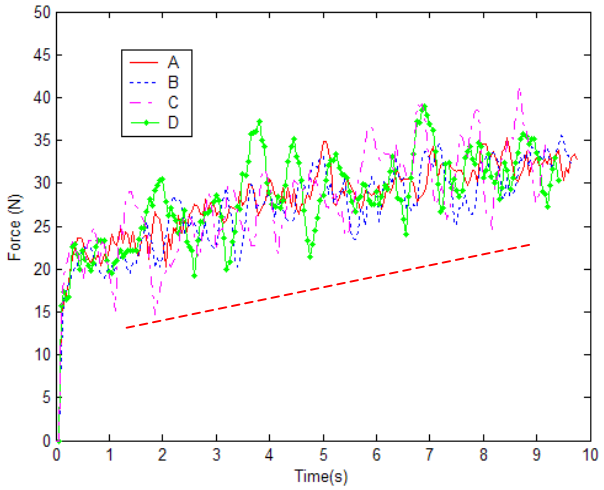


*Fig.5: Horizontal component force acting on the cutting-tool as a function of time in 2D simulation corresponding to four samples (A-D).*

### *3.2. Failure and resistance force in 3D*

The 3D simulation results will be discussed in this section in term of comparison between two simulation samples (G, H). Sample G was simulated with rake angle of 90 degree while sample H is that of 60 degree.

Figs.6 and 7 show the cross sectional images which were obtained at every 10mm interval with respect to the traveling distance of the cutting-tool from x=10mm to x=40mm. In these images, the deep region (failure zone) represents an area where particles took the large displacement comparing with their initial position, while the region of stationary particles is presented by the light color.

Fig.6 (a) shows the results of excavation using the cutting-tool with a rake angle of 90°. The cross section was taken at the plane where it is 60mm in width. From these images, it could be observed that the shape of boundary which divides deep color and light color (i.e., slip surface) changes from the curved line into the straight line during the progress of the blade, and the failure area of soil in front of the blade, deep region, increases with respect to the traveling distance of the blade. Fig.6 (b) shows the results of excavation for the cutting-tool with a rake angle of 60°. The images obtained in this case are similar to those of Case1, however comparing with Case1 as can be seen in the images of x = 10mm and x = 20mm, the shape of slip surface was first formed in the straight line and then it changes into the curved line while this is not found in Case1.

The cross sectional images in Fig.7 were obtained at a plane in front of the cutting-tool where it is 10mm far from the tip of the blade. Fig.7 (a) shows the results of excavation for the vertical blade (rake angle of 90°). From these images, it could be seen that the failure area increases with respect to the traveling distance of the cutting-tool. Moreover, comparing these images it could be observed that the failure area in front of the cutting-tool expands rapidly from the images of x = 10mm to x = 20mm, however this expansion becomes small afterward as seen in the images of x = 30mm and x = 40mm. This indicates that the failure area in front of the cutting-tool seems to be constant after some displacements of the cutting-tool. Fig.7 (b) shows the results for the inclined blade (rake angle of 60°). The images obtained in this case are similar to those of Case1. However, comparing with Case1 the failure area in front of the inclined blade seems to be smaller than that of the Case1.

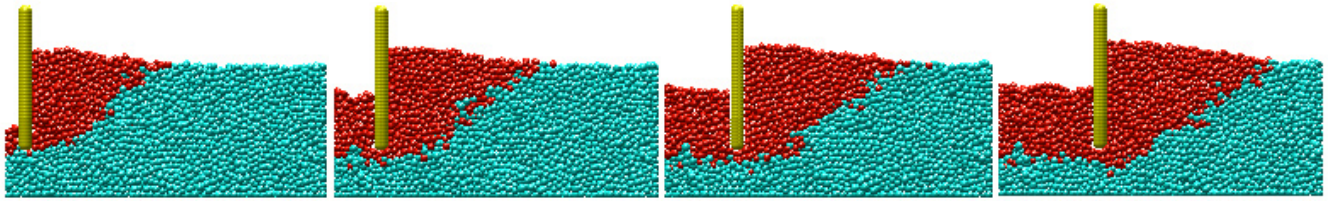

x = 10mm x = 20mm x = 30mm x = 40mm

(a) Case 1 (Rake angle: 90 deg, at 60mm in width)

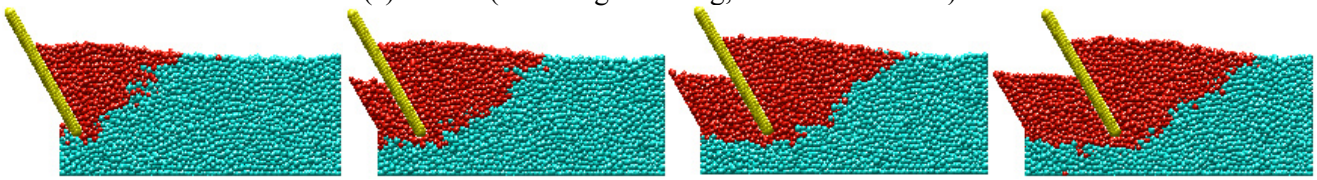

x = 10mm x = 20mm x = 30mm x = 40mm

(b) Case 2 (Rake angle: 60 deg, at 60mm in width)

*Fig. 6: Cross sectional images of failure length*

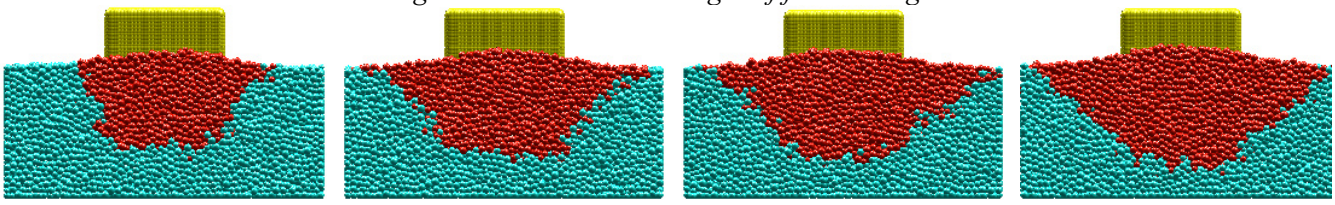

x = 10mm x = 20mm x = 30mm x = 40mm

(a) Case 1 (Rake angle: 90 deg, at 10mm in front of the blade)

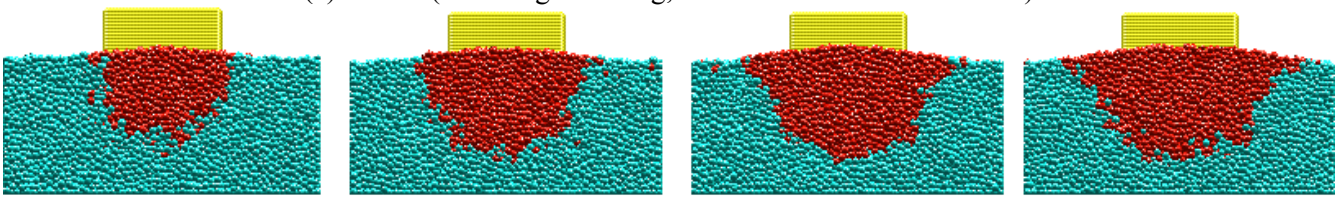

x = 10mm x = 20mm x = 30mm x = 40mm

(b) Case 2 (Rake angle: 60 deg, at 10mm in front of the tip of the blade)

*Fig.7: Cross sectional images of failure width*

Fig.8 shows the cross sectional images which were obtained at every 10mm interval with respect to the excavation depth from z = 10mm to 30mm. The first image was plotted at 5mm in depth in order to eliminate the effect of particles which fall down due to the growing up of soil particles in front of the blade. Fig.8 (a) presents the excavation using vertical blade while the excavation with inclined blade is presented in Fig.8 (b). From these images it could be seen that the section of boundary, which divides deep color and light color (i.e., slip surface), becomes curved and the failure region enclosed by the slip surface is enlarged as the ground surface is approached. Moreover, comparing between Case1 and Case2, as could be seen in the images of z = 5mm and z = 10mm, the angles of direction of slip surface from the excavation at the edge of cutting-tool seem to become wider for the Case1.

Fig.9 shows the 3D images of failure volume at the difference view when blade performed 30mm traveling distance. From these images, the three dimensional configuration of failure mechanism was clarified. The failure volume around the cutting-tool was enclosed by a curved line at the free surface. Moreover it could be seen that a curved slip surface has expanded from the blade tip to the ground surface in both case of simulations (incline blade and vertical blade).

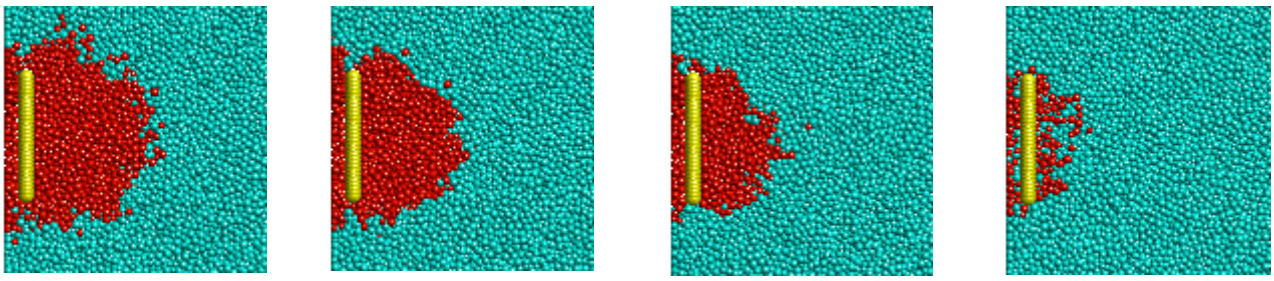

z = 5mm z = 10mm z = 20mm z = 30mm

(a) Case 1 (Rake angle: 90 deg, traveling distance: 10mm)

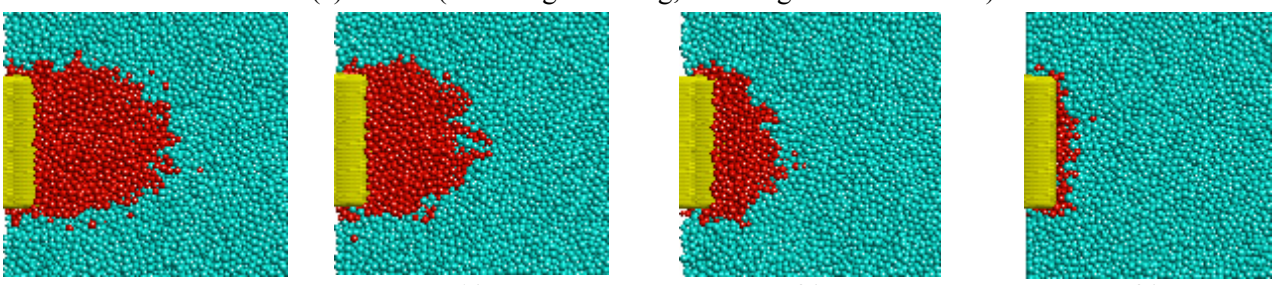

z = 5mm z = 10mm z = 20mm z = 30mm

(b) Case 2 (Rake angle: 60 deg, traveling distance: 10mm)

*Fig.8: Cross sectional images of failure depth*

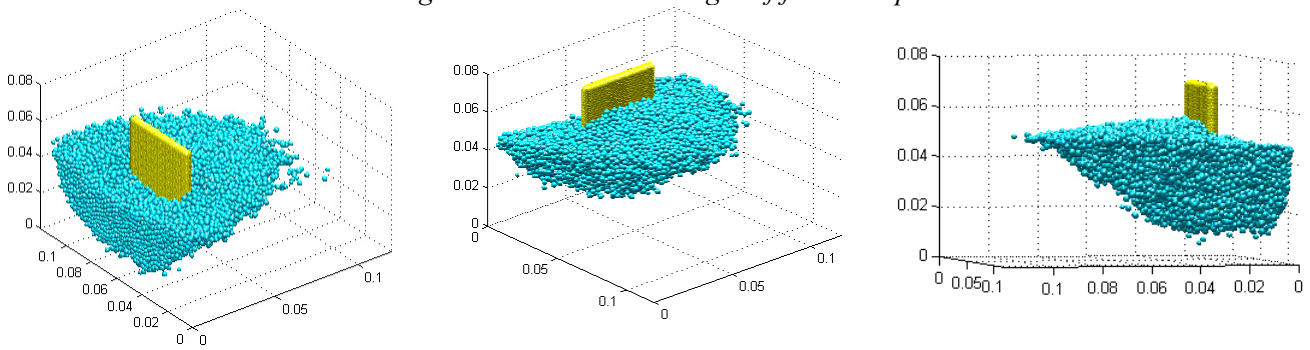

(a) Case 1 (Rake angle: 90 deg; Traveling distance: 30mm)

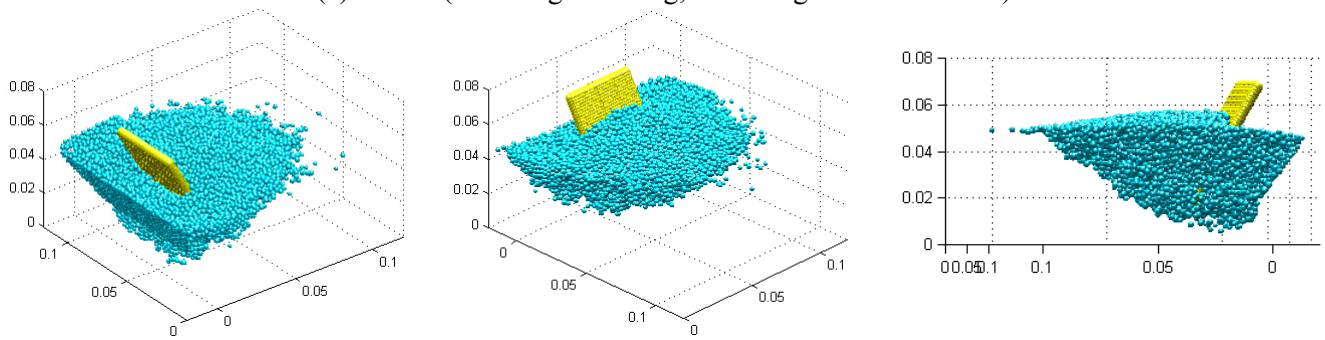

(b) Case 2 (Rake angle: 60 deg; Traveling distance: 30mm)

*Fig. 9: 3-D Images of failure mechanism*

Fig.10 shows the horizontal force acting on the cutting-tool for Case1 (rake angel of 90$^o$) and Case2 (rake angel of 60$^o$). Though this figure, each force tends to increase with irregular fluctuation with respect to time. Moreover, it could be seen that these forces increase rapidly in the fist interval of time but this increment becomes small afterward. This tendency also was observed in the failure width as shown in Fig.7 and it indicates that the force acting on the cutting-tool is proportional to the failure width of soil in front of the cutting-tool. Furthermore, comparing these forces in Fig.10 has shown that the force acting on inclined blade is smaller than the case of vertical blade.

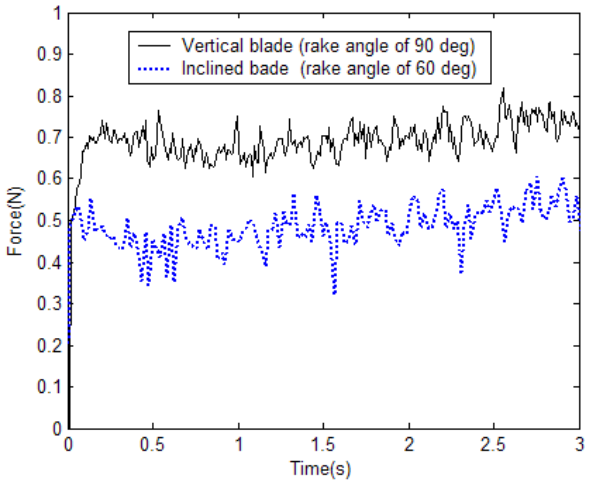


*Fig.10: Horizontal force acting on cutting-tool*

## 4. CONCLUSIONS:

The numerical investigation of soil excavation using Distinct Element Method (DEM) has been presented through this paper. Our study focuses on the shear deformation pattern and the resistance force acting on the cutting-tool. Calculation results have shown that:

The 2D simulation results agreed very well with the experiment in both mean of shear deformation pattern and resistance force acting on the cutting-tool. The slip surface change from the curve line into the straight line after each cycle where new slip line is

generated. The force acting on the cutting-tool has big fluctuation and this fluctuation is directly proportional to the size of particles. In spite of fluctuation, the mean force is independent of particle size and it is increased linearly with respect to the traveling distance of the cutting-tool.

In 3D, calculation results have shown that the cross sectional images of the excavation mechanism could be presented at any planes in DEM simulation. The failure width of soil in front of the cutting-tool expands rapidly in the first interval of time however this tendency becomes small afterward. Furthermore, the angle of the direction of slip surface from the excavation direction at the edge of the cutting-tool seems to become wider as the rake angle of the cutting-tool decrease, this result is also in agreement with the experimental results using X-ray radiography method conducted by Fukagawa, et al. [4]. In term of the excavation resistance, 3D simulation indicated that the force acting on the cutting-tool also has fluctuation and its magnitude become smaller as the rake angle of the cutting-tool decreases. In spite of linear increment in 2D simulation, the force seems to be constant after reaching the maximum value. This tendency was also found in the expansion of failure width of soil in front of the cutting-tool. Finally, the 3D failure mechanism of soil excavation could be visualized clearly from the DEM simulation.

REFERENCES


1. P. A. Cundall and O. D. L. Strack: *A discrete numerical model for granular assembles*, *Geotechnique, 29, No. 1, pp. 47-65, 1979.*
2. Ha. H. BUI, R. Fukagawa, T. Kobayashi and K. Tamoi: DEM simulation of three dimensional soil failure with cutting blade, Proc. of the 7th Asia-Pacific ISTVS Conference, Changchun, China, September 2004.
3. Ha H. BUI. Numerical Simulation of Excavation with Cutting-Blade by DEM, Master Thesis, Ritsumeikan University, 2004.
4. R. Fukagawa, T. Kobayashi, K. Tateyama and H. Takahashi: Three dimensional visualization of the excavation mechanism for dry sandy ground by a CT-scan technique, Proc. of the 9th European Conference of the ISTVS, 9, Harper Adams, UK, pp. 128-135, 2003.
5. E. T. Selig and R. D: Nelson, Observation of Soil Cutting with Blade, Journal of Terramechanics, Vol. 13, pp. 32-53, 1964.